# Optimized Trajectory Tracking of a Class of Uncertain Systems Applied to Optimized Raster Scanning in Near-Field Measurements

**AMEDEO CAPOZZOLI, (Member, IEEE), LAURA CELENTANO, (Member, IEEE), CLAUDIO CURCIO, ANGELO LISENO, AND SALVATORE SAVARESE**

Department of Electrical and Information Technology, University of Naples Federico II, 80125 Napoli, Italy

Corresponding author: Laura Celentano (laura.celentano@unina.it)

**ABSTRACT** A tracking problem is considered for a very recurring class of systems, such as Cartesian robots with real actuators, conveyor belts, and certain scanning devices used for medical and engineering applications, as near-field antenna characterization. Theorems are proven for the design of a PID controller with a possible compensation signal to track sufficiently regular trajectories with a prescribed maximum error. The developed design methodology is used to identify the current antenna scanning system without a controller and to design and construct a new controller that provides better performance than the current one. Moreover, this paper proposes an optimized raster scan acquisition scheme that reduces the number of field samples and the scanning path length compared with the more conventional approaches. By using the new controller and the proposed optimized sampling strategy, which provides a sparse distribution of the samples, the performance of an antenna can be evaluated in a considerably shorter time than that necessary using the pre-existing controller and standard scanning, as experimentally assessed in this paper.

**INDEX TERMS** Robust controller design, robust tracking, uncertain nonlinear systems, positive control systems, near-field antenna measurements, antenna scanning system, optimized raster scanning.

## I. INTRODUCTION

Near-field (NF) antenna measurements [1] are an established solution to antenna pattern characterization. They require the measurement of field data on a scanning surface located in the near-field region of the antenna under test (AUT). The AUT is typically far enough from the source that the contributions to the measured field of the invisible portion of the spectrum are vanishingly small. Generally, the geometry of the scanning surface hosting the sampling points where the field samples are collected is planar, cylindrical or spherical. Each solution shows advantages and drawbacks depending also on the characteristics of the AUT and on the system where it is installed [2]. After the collection of near-field data, the far-field (FF) is calculated according to a NF-FF transformation.

In recent years, many efforts have been made to solve a very relevant issue that affects NF measurements related to the large amount of field samples that must be collected on the scanning surface to make the NF-FF transformation accurate [3]–[9]. Indeed, the amount of data and the scanning path length in particular affect the time required to complete the acquisition, which can be particularly long. However, the scanning time is determined not only by the number of field samples to be collected but also by the scanning path length. Typically, three directions can be pursued to reduce the acquisition time and to preserve the accuracy of FF predictions:

1. The characteristics of the employed hardware can be improved: in practice, the velocity of the probe can be increased by using measurement instruments with better performance and reduced latencies.
2. The field samples can be reduced in number and sparsely distributed along the scanning path [10], and the scanning path length can be shortened: sparse distribution of the samples allows for faster movements between two consecutive sampling points, profiting of the scanner capabilities and disregarding for the measurement instrument latency.
3. The algorithm controlling the hardware can be improved by exploiting an efficient and effective approach that takes advantage of both the available hardware and the sampling strategy.

A. Capozzoli *et al.*: Optimized Trajectory Tracking of a Class of Uncertain Systems Applied to Optimized Raster Scanning

IEEE *Access*

Clearly, successfully acting on the three points above requires different competencies. However, in practice, the adopted solutions in the three areas influence each other and require a strict interaction among the designers of the measurement setup.

This paper focuses on the last two points above. The hardware is assumed predetermined because it is already available. Furthermore, a new approach is presented that speeds up the NF acquisitions and cultivates a successful synergy between an optimized sampling strategy and an optimized control approach. From the electromagnetic theory point of view, the optimized sampling strategy is based on the concept of singular value optimization (SVO) [4]–[8]. SVO has recently been proven to determine the number and distribution of the NF samples by dramatically reducing the sampling rate and the scanning path length without sacrificing accuracy. In this paper, for the first time, SVO returns a new (optimized) raster data collection that requires a single-axis continuous acquisition driven by a smart controller. Indeed, the scanning area is covered as the composition of an optimally selected row, hosting samples non-uniformly spaced according to a row-wise optimality condition. The raster scan has been specifically conceived to profit from a simple but effective handling of the hardware, drawn from the flexibility of the powerful SVO. The approach allows a large distance between sampling points compared to competitors and frees space for the controller for large accelerations between consecutive sampling points to significantly reduce the scanning time.

Accordingly, from the control theory viewpoint, the problem requires the design of a controller that can profit at the best from both the sparsity of the field measurements and the available hardware.

It is worth noting that this control problem is shared with other disciplines, since many electro-mechanical, thermal, chemical, biological and medical linear and nonlinear systems exist, which are subject to parametric uncertainties and have non-standard disturbances, that need to be efficiently controlled. For these systems, robust and simple controllers that can track quickly with the prescribed precision and non-standard references must be designed and constructed.

Numerous scientific papers addressing this goal are available in the literature, also very recent, which propose adaptive sliding mode controllers, feedback linearization and fuzzy control techniques applied to theoretical and engineering problems (e.g., [11]–[20]).

Some robust tracking methods for uncertain linear and nonlinear MIMO systems of realistic trajectories have also been provided by Celentano [21]–[24].

However, in the literature, the following practical limitations remain for several cases:
- the considered references and disturbances are often standard waveforms (polynomial and/or sinusoidal ones);

- the control signals are in some cases excessive and/or unfeasible because of chattering;
- the actuators are assumed to be ideal.

In this paper, new and useful theorems are provided, which allow to easily design a robust PID control law with a possible compensation signal and without chattering. This controller is used to force an uncertain third-order system with additional nonlinearities and/or disturbances to track a preassigned trajectory, with bounded third derivative, with a predetermined maximum error.

The main contributions of these new results to the control theory presented in this paper consist of the following:
- the considered class of systems that need to be controlled is very common in practice; some examples include Cartesian robots with real actuators and several transportation systems;
- the control law is easy to design and implement;
- the trajectory to track can have generic behavior, provided that its third derivative is bounded;
- suitable filtering laws of the trajectory to track and/or some techniques useful to choose the reference signal are provided, to make the implementation of the controller easier and to reduce the control signal, above all during the transient phase;
- the predetermined maximum error is guaranteed despite uncertainties, bounded nonlinearities and/or bounded disturbances;
- a very easy relationship between a single design parameter of the controller and the maximum tracking error is provided, which is useful to obtain the desired tracking precision.

In addition, the notable utility of this work for industrial purposes clearly emerges from the presented application; i.e, a significant class of electro-mechanical systems can be effectively controlled analogously, via an easily designed and constructed controller, to track sufficiently regular trajectories with high precision.

The developed design methodology is used to identify, design and construct a scanning system used together with an optimized raster sampling to speed up the acquisition process in a planar NF antenna characterization. Several experimental validation tests and useful applications have been made at the Microwave and Millimeter Wave Laboratory at University of Naples Federico II.

The paper is organized as follows. In Section II, the measurement process is placed in a general mathematical framework that makes the application of the SVO concept straightforward. In Section III, the NF acquisition based on SVO is summarized, while the new optimized raster sampling strategy is illustrated in Section IV. In Section V, the new control theory to design the control system of the NF scanner is presented. In Section VI, the general controller design is provided. In Section VII, the design, realization and validation of the controller for the antenna scanning system is presented. Some results of the experimental testing campaign

IEEE Access

A. Capozzoli *et al.*: Optimized Trajectory Tracking of a Class of Uncertain Systems Applied to Optimized Raster Scanning

are reported in Section VIII, where the performance of the proposed approach is compared with that of standard scanning, showing significant improvements. Conclusions and future developments follow in Section IX.

## II. THE MEASUREMENT PROCESS

As mentioned in the Introduction, one of the key points to speed up the acquisition process in NF measurements comes from the definition of a convenient sampling point number and distribution that minimizes the scanning path length and the number of samples located therein.

In this section, the concepts underlying the field measurements are presented. The probe is assumed to not interact with the AUT because of mutual couplings or with the surrounding environment.
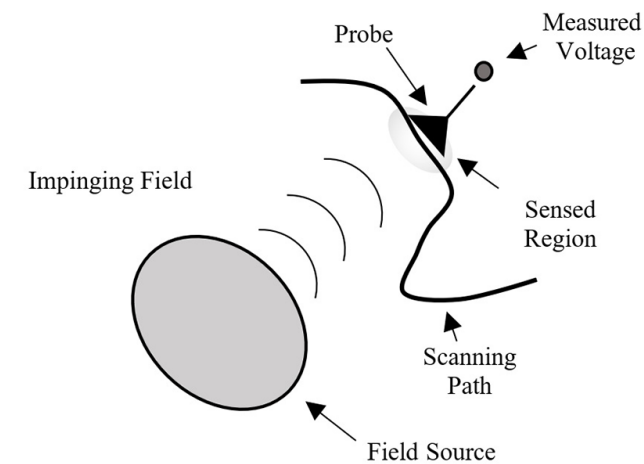


**FIGURE 1.** Schematic representation of the measurement process.

The schematic representation of the measurement process is presented in Fig. 1. A source radiates the field, and a probe antenna is moved along a trajectory on the scanning surface to collect the information available therein. The information is carried out by the impinging field, i.e., the field produced by the radiator all over the sensing region when the probe is absent. In particular, for each probe position, the information is extracted from the field in the region sensed by the probe, and a voltage is made available to the users by the measurement instrument.

As long as the probe antenna is made of linear materials and linear components, in the phasor representation, the relationship between the impinging field in the sensed region, represented by a complex vector field, say $\underline{E}_s$, and the voltage acquired by the instruments, which is typically a vector network analyzer (VNA), say $v_0$, is expressed by a linear functional $\mathcal{M}$

$$\mathcal{M}|\underline{E}_s \to \mathcal{M}\left(\underline{E}_s\right) = <\underline{E}_s, \underline{M}> = v_0. \quad (1)$$

In eq. (1), the symbol $<, >$ denotes the duality, representing the linear functional in terms of a vector field $\underline{M}$ in the dual space of that containing $\underline{E}_s$ [25]. $\mathcal{M}$ represents the measurement process and accounts for the probe/instruments response and the probe location.

To obtain $v_0$ from $\underline{E}_s$, $\underline{E}_s$ should be known all over the sensed region, which in practice is the region occupied by the probe. In fact, the voltage $v_0$ can be determined only if the total field is known at the probe terminals, i.e., the superposition of the field $\underline{E}_s$ impinging on the probe and the scattered one. The total field can be determined after solving the scattering problem for the probe; to this end, the characteristics of the probe and $\underline{E}_s$ on the whole body of the antenna are required.

## III. THE NF ACQUISITION STRATEGY BASED ON THE SVO

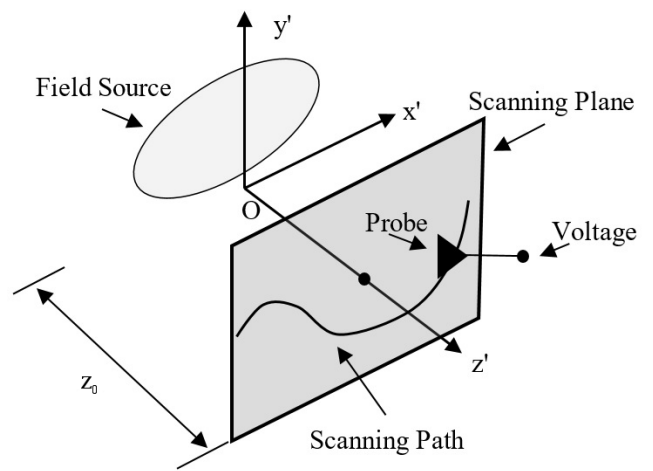In this section, the optimized NF/FF transformation based on SVO is briefly illustrated.



**FIGURE 2.** Geometry of a Planar NF acquisition system.

Consider the case of a planar scanner for NF measurements. The geometry of the system is depicted in Fig. 2. The general bounded field source is assumed in the half-space $z' \leq 0$, while the scanning plane where the probe (probes) must be located is assumed to be the plane $z' = z_0$. The scanning plane is assumed to be located outside of the reactive region of the source to have negligible contributions of the invisible part of the plane wave spectrum to the field therein.

According to the plane wave expansion theorem [26], the field in the half-space $z' \geq z_0$, say $\boldsymbol{H}$, is completely determined once the tangent components of the E-field on the scanning plane, say $\underline{E}_d$, are given. Then, as long as the probe is embedded in $\boldsymbol{H}$, touching the scanning plane, the sensed field $\underline{E}_s$ is completely determined by $\underline{E}_d$.

Accordingly, eq. (1) turns into

$$\mathcal{M}|\underline{E}_d \to \mathcal{M}\left(\underline{E}_d\right) = <\underline{E}_d, \underline{M}> = v_0. \quad (2)$$

In the formal framework introduced here, the measurement process turns into the selection of a finite set (the measurement process involves the collection of a finite number of voltages) of functionals $\mathcal{M}$ (or equivalently $\underline{M}$). Such functionals make it possible to retrieve sufficient information to

A. Capozzoli *et al.*: Optimized Trajectory Tracking of a Class of Uncertain Systems Applied to Optimized Raster Scanning

**IEEE** *Access*

calculate the FF radiated by the source in the directions in $H$. This set of Q functionals, say $\{\underline{M}_q\}_{q=1}^Q$, can represent different probes exploited to sense the field to extract independent features of $\underline{E}_d$, or the same probe moving with the same end, along the scanning path. The second solution is the one typically adopted since it allows the use of small probes with a limited impact on the coupling between the probe itself and the radiating system. The different functionals correspond to different acquisition processes, which in turn correspond to the voltage measurements for different probe locations. In this case, for an ideal probe that picks up the value of the field in a point along a direction, $\underline{M} = \underline{m}\delta(\underline{r} - \underline{r}_m)$, where $\underline{m}$ identifies the measured component direction of the field and the conversion factor of probe/instrument, $\delta$ represents the Dirac pulse, and $\underline{r}_m$ is the position where the field is measured. The operator $\mathcal{R}$ is now introduced and maps the quantities that describe the radiative characteristics of the radiator, say $\underline{J}$, to $\underline{E}_d$. Depending on the case, the vector field $\underline{J}$ can represent equivalent currents (magnetic or electric according to the adopted formulation) or the field components tangent to the source envelope. $\underline{J}$ is assumed to belong to a finite dimensional linear space, say $\boldsymbol{J}$, with minimum dimension $N$, that is relevant to evaluate both $\underline{E}_d$ and the FF, in all the conditions of interest [4].

Accordingly, eq. (2) turns into

$$\mathcal{A}|\underline{J} \in \boldsymbol{J} \rightarrow \mathcal{M}\left(\mathcal{R}(\underline{J})\right) = < \mathcal{R}(\underline{J}), \underline{M} > = v_0. \quad (3)$$

Once a set of basis functions for $\boldsymbol{J}$ is introduced, say $\{\underline{J}_n\}_{n=1}^N$, $\underline{J}$ can be written as $\underline{J} = \sum_{n=1}^N \alpha_n \underline{J}_n$ and eq. (3) becomes

$$v_0 = \sum_{n=1}^N \alpha_n < \mathcal{R}(\underline{J}_n), \underline{M} > . \quad (4)$$

The antenna characterization amounts to find the vector $\underline{\alpha}$ of the coefficients $\alpha_n$, given a vector of Q voltages (corresponding to the set of Q measurement functionals), say $\underline{b}$. Indeed, given $\underline{\alpha}$ and thus $\underline{J}$, the FF can be easily calculated by standard formulas from the electromagnetic theory [4].

In other words, unlike what is typical, the NF antenna characterization can be recast as a linear inverse problem on finite dimensional linear sub-spaces

$$\underline{b} = \underline{\underline{A}} \cdot \underline{\alpha}, \quad (5)$$

where $\underline{\underline{A}}$ is the matrix whose entries are

$$A_{qn} = < \mathcal{R}(\underline{J}_n), \underline{M}_q > . \quad (6)$$

The inversion of $\underline{\underline{A}}$ is typically ill-conditioned. However, one degree of freedom is still available since the functionals $\underline{M}_q$ are still free to be selected to improve the singular value behavior of $\underline{\underline{A}}$. Indeed, the measurement processes can be devised to select the matrix among all the possible matrices $\underline{\underline{A}}$ that is the most convenient since it is the best conditioned thanks to SVO. In this sense, the SVO is a regularization algorithm, and the measurement process turns into preconditioning. The residual ill-conditioning can be cured using a regularization approach, as the truncated singular value decomposition (SVD) or the L-curve method [27].

The optimization of the singular values behavior is performed here without accounting for the power level signal through the optimization of the function

$$\Psi = \sum_{k=1}^K \frac{\sigma_k}{\sigma_1}, \quad (7)$$

where $\sigma_k$ are the singular values of $\underline{\underline{A}}$, in decreasing order. $\Psi$ is known as the Shannon number and provides a "measure" of the information about $J$ extracted from the field [4]. The optimal Q is obtained from an iterative procedure based on the assumption that no more information can be extracted beyond a certain value of Q [28]. Note that the functional in eq. (7) is always positive since the singular values of a matrix are non-negative and the singular values are not identically vanishing.

## IV. THE OPTIMIZED RASTER SCAN ACQUISITION FOR APERTURE ANTENNAS

The general approach summarized above is here, for the first time, exploited for the optimized raster acquisition scheme in the case of aperture antennas.

The raster scanning acquisition is considered here instead of the quasi raster one [8] since it simply allows a one-dimensional smart control of the probe continuous movements that profit at the best of the hardware capabilities and of the sparse distribution of the sampling points. In particular, the sparse distribution is along the horizontal axis (rows), and only simple step motions along the vertical axis (columns) are required.
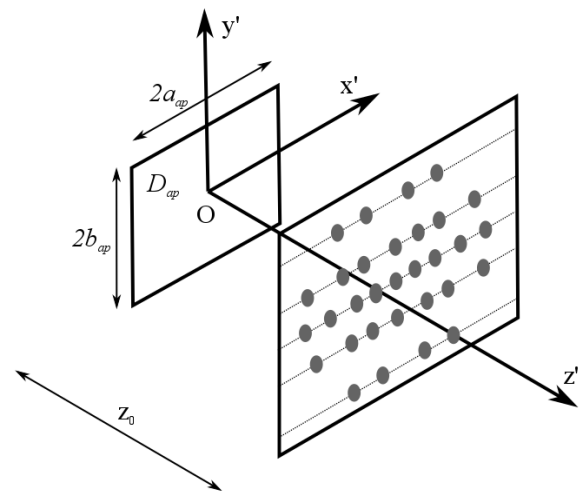


**FIGURE 3.** Geometry of the optimized raster acquisition for aperture antennas.

In this case, the source of the field is assumed to be a rectangular aperture $D_{ap}$ with dimensions $2a_{ap} \times 2b_{ap}$ centered in the $Ox'y'z'$ reference system (Fig. 3). As before, the field is assumed to be measured on the plane, located a distance $z_0$ apart from the aperture. In Fig. 3, the gray dots represent the field sampling points.

For the sake of brevity and without loss in generality, a scalar case is considered with a linearly polarized aperture field so that $\underline{E}_a = E_a\hat{y}$. $\underline{E}_a$ takes on here the role of $\underline{J}$ in the general description presented in Section III. The probe is assumed to be electrically small and linearly polarized so that its correction can be deemed irrelevant. In this way, the SVO determines the optimal number and spatial distribution of the sampling points.

The finite dimensional linear sub-space $\mathcal{J}$ containing the aperture field can be easily identified once it is observed that the aperture field, which is relevant to determine both the component of $\underline{E}_d$, say $E_d$, and the FF Pattern (FFP), is a function with bounded support, and band limited. Then, the prolate spheroidal wave functions [29] can be exploited as basis functions of $\mathcal{J}$ so that

$$E_a(x', y') = \sum_{p=1}^{P}\sum_{g=1}^{G} a_{pg}\Phi_p[x', c_x]\Phi_g[y', c_y], \quad (8)$$

where $\Phi_i[w, c_w]$ is the i-th 1D prolate spheroidal wave function with "space-bandwidth product" $c_w$, $c_x = a_{ap}k_{x0}$, $c_y = b_{ap}k_{y0}$, and $k_{x0}$ and $k_{y0}$ locate the spectral region of interest. In eq. (8) $P = \text{Int}[4a_{ap}/\lambda]$ and $G = \text{Int}[4b_{ap}/\lambda]$, where $\lambda$ is the wavelength.

Concerning its formal expression, the radiation operator $\mathcal{R}$ can be easily written based on the plane wave expansion theory. Plane wave expansion theory enables representing the field in the half-space $z \geq 0$ as a superposition of plane waves, as detailed in [26]. Accordingly,

$$E_d(x', y') = \iint_{\mathbb{R}^2} dk_x dk_y \widehat{E}(k_x, k_y)e^{-j(k_x x' + k_y y' + k_z z_0)}, \quad (9)$$

where R is the set of real numbers, $k_z = \sqrt{\beta^2 - (k_x^2 + k_y^2)}$, and $\widehat{E}$ is the $y'$-component of the plane wave spectrum

$$\widehat{E}(k_x, k_y) = \frac{1}{(2\pi)^2}\iint_{D_{ap}} dx' dy' E_a(x', y')e^{j(k_x x' + k_y y')}. \quad (10)$$

The entries of the matrix $\underline{\underline{A}}$ can be easily calculated from eqs. (8-10).

The optimized sampling should provide a rectangular raster acquisition scheme, wherein a proper spacing of the acquisition rows and a sparse (non-uniform) sampling point with a distribution on each row is considered. Indeed, sparsity allows an increased acquisition speed, even in continuous scanning. Unlike what is commonly done, after using a proper control strategy, the continuous movement of the probe can be performed at variable velocity. The minimum velocity is fixed by the latency of the measurement instrument. The maximum velocity is imposed by the controller capabilities, by the accuracy required in the positioning and by the hardware characteristics of the scanner. In other words, the latency of the VNA, even if externally triggered, forces an upper bound to the velocity of the probe movement during the acquisition of the field sample. However, a powerful control system can

move the probe along a trajectory that is non-uniformly traveled, accelerating and decelerating between two field sampling points, to take full advantage of the reduced sampling grid and to significantly increase the average speed between two consecutive measurements.
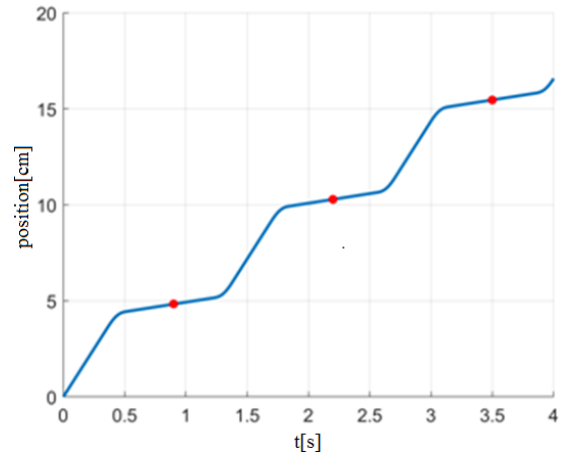


**FIGURE 4.** Trajectory traversing three sampling points (red dots) with varying speed.
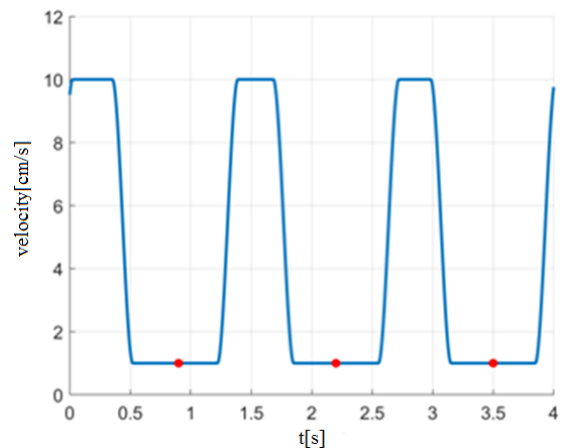


**FIGURE 5.** Illustration of the velocity behavior associated with a trajectory traversing three sampling points.

To better illustrate this point, Figs. 4 and 5 show a trajectory traversing the three samples on a row (depicted in red) and the corresponding velocity behavior, respectively. In the neighborhood of the sampling points, the probe can move according to the VNA requirements. Then, after the acquisition, the velocity is increased as much as possible to quickly reach the next point.

The boost in the acquisition speed is obviously larger as the sparsity of the sampling points increases. Opposite to that, if the distribution of sampling points along the rows is a standard uniform one, then the accelerations of the probe motion can be faint and useless.

In the newly introduced sampling strategy, based on SVO, the row locations are expressed as

$$y_i' = \sum_r c_r P_r(\eta_i), \quad (11)$$

where the $P_r$ are proper basis functions (e.g., Legendre polynomials), the $c_r$ are expansion coefficients, and the $\eta_i$ are uniformly spaced in $[-1, 1]$. Moreover, along each row, the non-uniform sample locations are expressed as

$$x'_{ij} = \sum_r d_r \left(y'_i\right) P_r \left(\xi_j\right), \tag{12}$$

where the $d_r$ are expansion coefficients, and the $\xi_i$ are again uniformly spaced in $[-1, 1]$. Note that the expansion coefficients $d_r$ now depend on the row. The resulting grid allows a non-uniform raster acquisition with a continuous scan of the horizontal axis.

SVO is exploited to determine the coefficients $c_r$ and $d_r$.

## V. FORMULATION OF THE CONTROL PROBLEM

The problem of defining the control system is now approached. In this section, a new control theory is provided, and in the subsequent ones, its application to the considered problem is reported.

Consider the nonlinear uncertain dynamic system:

$$\dot{y} = v$$
$$\ddot{v} + a_1(p)\dot{v} + a_2(p)v = b(p)u + f(t, y, v, p, d), \tag{13}$$

where $t \in \mathcal{T} = [0, t_f] \subset R$ is the time, $y \in Y \subset R$ is the output, $v \in V \subset R$ is the rate of variation in the output $y$, $u \in U \subset R$ is the input, $d \in D \subset R$ is the disturbance, $p \in \wp \subset R^\mu$ is the vector of uncertain parameters, $f \in R$ is a nonlinear bounded function and $r(t) \in R$ is the reference signal with bounded third derivative.

Assume that:

$$a_1(p) \in \left[a_1^-, a_1^+\right], \quad a_1^- > 0, \ a_2(p) \in \left[a_2^-, a_2^+\right],$$
$$b(p) \in \left[b^-, b^+\right], \quad b^- > 0, \ |f(t, y, v, p, d)| \leq \hat{f}, \tag{14}$$
$$\forall t, y, v, p, d \in \mathcal{T} \times Y \times V \times \wp \times D, \ \hat{f} \geq 0,$$

and that $y$ is measurable.

The aim is to design a control law of the following type

$$u = K_p e + K_i \int e(\tau)d\tau + K_d \dot{e} + u_c(t, y, v, r, \dot{r}, \ddot{r}, r), \tag{15}$$

where $e = r - y$ is the tracking error, and $u_c$ is a possible compensation signal, such that the maximum of the absolute value of the tracking error $e_M = \max_{t \in \mathcal{T}} |e(t)|$ is not higher than a prefixed value.

The class of systems (13) is very common in practice. Some examples include the Cartesian robots with real actuators, several transportation systems, some electromechanical systems and electro-hydraulic systems, some scanning devices for medical and engineering applications, and some systems whose output is a variable physical quantity.

As a second remark, it is stressed that a reference signal $r(t)$ with its bounded third derivative can be obtained by interpolating a set of given points $(t_k, r_k)$, $k = 0, 1, \ldots, n$, via cubic

splines or by filtering any piecewise constant or piecewise linear signal $\tilde{r}(t)$ with a suitable fourth-order filter:

$$\dot{\varphi} = \begin{bmatrix} 0 & 1 & 0 & 0 \\ 0 & 0 & 1 & 0 \\ 0 & 0 & 0 & 1 \\ -f_4 & -f_3 & -f_2 & -f_1 \end{bmatrix} \varphi + \begin{bmatrix} 0 \\ 0 \\ 0 \\ f_4 \end{bmatrix} \tilde{r},$$

$$\varphi = \begin{bmatrix} r \\ \dot{r} \\ \ddot{r} \\ r \end{bmatrix}. \tag{16}$$

It is worth noting that if the filter is a Bessel with a cutoff angular frequency $\omega_b$ greater or equal to the angular frequency of $\tilde{r}(t)$, then (see [23], [24]) $r(t) \cong \tilde{r}(t - t_r)$, $t_r = \pi/\omega_b$.

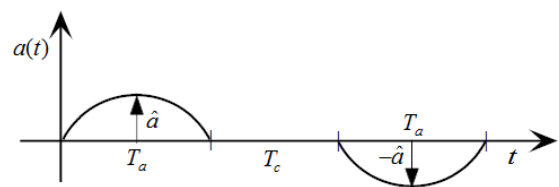For mechanical systems, the following theorem is useful.



**FIGURE 6.** Time history of the acceleration.

*Theorem 1:* Let $\hat{v}$ and $\hat{a}$ be the maximum values that the velocity and acceleration can reach, respectively. The minimum time $T_m$ for traveling a distance $S$ with a velocity $v \leq \hat{v}$, $v(0) = 0$, $v(T_m) = 0$ and an acceleration $|a| \leq \hat{a}$, with quadratic acceleration and deceleration phases as in Fig. 6, is $T_m = 2T_a + T_c$, where:

$$T_a = \frac{3\hat{v}}{2\hat{a}}, \quad T_c = \frac{S - S_a}{\hat{v}}, \quad \text{if } S_a = \frac{3\hat{v}^2}{2\hat{a}} < S \tag{17}$$

$$T_a = \sqrt{\frac{3S}{2\hat{a}}}, \quad T_c = 0, \quad \text{if } S_a = \frac{3\hat{v}^2}{2\hat{a}} \geq S. \tag{18}$$

*Proof:* The proof of the theorem and an algorithm to compute $a(t)$, $v(t) = \int_0^t a(\tau)d\tau$, $s(t) = \int_0^t v(\tau)d\tau$ easily follow by noting that for assigned values of $T$ and $V$:

$$a(t) = -\frac{6V}{T^3}\left(t^2 - Tt\right), \quad t \in [0, T],$$

$$\Rightarrow \max a(t) = \hat{a} = \frac{3V}{2T}$$

$$v(t) = -\frac{V}{T^3}\left(2t^3 - 3Tt^2\right) \Rightarrow v(T) = V$$

$$s(t) = -\frac{V}{T^3}\left(\frac{t^4}{2} - Tt^3\right) \Rightarrow s(T) = \frac{VT}{2}. \tag{19}$$

The availability of $\dot{r}(t)$, if $\dot{y} = v$ is measurable, allows avoiding the derivative action of the controller; this is necessary when the measure of $y$ is noisy in the bandwidth of the system to control and/or when a real PID can considerably reduce the control system performance.

Furthermore, to drive the transient and/or to reduce the control action, above all during the transient phase, the initial conditions of the filter and its cutoff frequency can be

suitably chosen or a suitable connecting trajectory $r_j$, $\dot{r}_j$ can be considered.

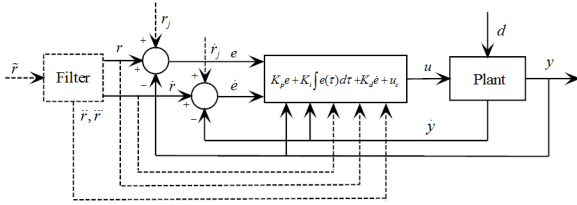Based on the previous considerations, a possible scheme of the control system is reported in Fig. 7.

**FIGURE 7.** Control system scheme.

To design the controller (15) the lemmas reported in the Appendix are necessary.

## VI. CONTROLLER DESIGN

It is easy to verify that the closed-loop control system (13) and (15) can be characterized by the following equation

$$e + a_1 e + \gamma_2 \ddot{e} + \gamma_3 \dot{e} + \gamma_4 = \dot{\zeta} = \zeta_p, \qquad (20)$$

where:

$$\gamma_2 = bK_d + a_2, \quad \gamma_3 = bK_p, \quad \gamma_4 = bK_i$$
$$\zeta = r + a_1 \ddot{r} + a_2 \dot{r} - f - bu_c. \qquad (21)$$

The following two results hold and are crucial to the design of the control system.

*Theorem 2:* Given system (13) without parametric uncertainties and controller (15) with gains $K_p$, $K_i$ and $K_d$ such that the roots of the polynomial

$$p(s) = s^4 + a_1 s^3 + \gamma_2 s^2 + \gamma_3 s + \gamma_4$$
$$= s^4 + a_1 s^3 + (bK_d + a_2)s^2 + bK_p s + bK_i \quad (22)$$

are $-\frac{a_1}{4}, -\frac{a_1}{4}, -\frac{a_1}{4} \pm j\omega$, $\omega \geq 0$, then, except for a possible transitory, the error of the control system satisfies the following inequality

$$|e(t)| \leq H\delta_p, \quad H = \frac{1}{a_1^2/16(a_1^2/16+\omega^2)}, \quad \delta_p = \max\left|\dot{\zeta}\right| \qquad (23)$$

or

$$|e(t)| \leq H_p \delta, \quad H_p = \frac{1}{a_1/4(a_1^2/16+\omega^2)}, \quad \delta = \max|\zeta|. \qquad (24)$$

*Proof:* The proof easily follows from Lemmas 2 and 3 in the Appendix.

*Theorem 3:* Given the control system (13) and (15), choose the gains $K_p$, $K_i$ and $K_d$ such that the roots of the polynomial

$$p(s) = s^4 + \bar{a}_1 s^3 + \bar{\gamma}_2 s^2 + \bar{\gamma}_3 s + \bar{\gamma}_4$$
$$= s^4 + \bar{a}_1 s^3 + (\bar{b}K_d + \bar{a}_2)s^2 + \bar{b}K_p s + \bar{b}K_i \quad (25)$$

are $-\frac{\bar{a}_1}{4}, -\frac{\bar{a}_1}{4}(1 - \varepsilon), -\frac{\bar{a}_1}{4} \pm j\omega$, and where $\bar{a}_1 = a_1(\bar{p})$, $\bar{a}_2 = a_2(\bar{p})$, $\bar{b} = b(\bar{p})$, $\bar{p}$ are the nominal values of $\{a_1, a_2, b, p\}$, $\omega \geq 0$ and $\varepsilon \in (0, 1)$. Then if

$$p(s, a_1, a_2, b) = s^4 + a_1 s^3 + (bK_d + a_2)s^2 + bK_p s + bK_i \qquad (26)$$

is a Hurwitz polynomial $\forall a_1 \in [a_1^-, a_1^+]$, $\forall a_2 \in [a_2^-, a_2^+]$, $\forall b \in [b^-, b^+]$, except for a possible transitory, it is:

$$|e(t)| \leq H\delta_p, \quad \delta_p = \max\left|\dot{\zeta}\right|$$

$$H = \max_{\substack{a_1 \in [a_1^-, a_1^+] \\ a_2 \in [a_2^-, a_2^+] \\ b \in [b^-, b^+]}} \left( \int_0^\infty \left| L^{-1}\left( \frac{1}{p(s, a_1, a_2, b)} \right) \right| d\tau \right) \qquad (27)$$

or

$$|e(t)| \leq H_p \delta, \quad \delta = \max|\zeta|$$

$$H_p = \max_{\substack{a_1 \in [a_1^-, a_1^+] \\ a_2 \in [a_2^-, a_2^+] \\ b \in [b^-, b^+]}} \left( \int_0^\infty \left| L^{-1}\left( \frac{s}{p(s, a_1, a_2, b)} \right) \right| d\tau \right). \qquad (28)$$

*Proof:* The proof follows from Lemmas 2 and 3.

Now, some interesting remarks are provided.

*Remark 1:* By considering (23), (24), (27), and (28), the tracking error can be reduced by increasing $\omega$ and/or, if necessary, reducing $\delta$ by using an appropriate compensation signal e.g. of type

$$u_c = \frac{r + a_1(\bar{p})\ddot{r} + a_2(\bar{p})\dot{r} - f(t, y, v, \bar{p}, \bar{d})}{b(\bar{p})}, \qquad (29)$$

where $\bar{p}$, $\bar{d}$ are the nominal values of $p$, $d$. In the hypothesis of not excessive parametric variations, it follows that the gain $H(H_p)$ can be made much smaller, and hence, the tracking error can be made as small as desired, even without the compensation $u_c$.

*Remark 2:* The computation of $H$ via (27) or $H_p$ via (28) can be easily made, for instance, with the MATLAB command *fmincon*.

*Remark 3:* If the desired precision cannot be obtained due to high parametric variations, to have a prescribed maximum tracking error, it is possible to do the following:

- better identify the system to be controlled (13) so that to reduce the uncertainty interval of the parameters $a_1, a_2, b$;
- increase $a_1$ by varying, if it is possible, some parameters of the system to be controlled or by introducing additional control action of the type: $K_{dd}\ddot{e} = K_{dd}(\ddot{r} - \dot{v})$, where $\dot{v}$ can be obtained through a real derivative if the measurement of $v$ is slightly noisy or through an additional sensor;
- in the case of the electro-mechanical systems, add a control action of the type $-K_R i$, where $i$ is the current absorbed by the motor, or increase the resistance $R$ of the motor if there are no energy performance problems;

A. Capozzoli *et al.*: Optimized Trajectory Tracking of a Class of Uncertain Systems Applied to Optimized Raster Scanning

**IEEE** *Access*

- reduce the reference signal variability by a suitable time scale factor, i.e., by considering as a reference the signal $r_\rho(t) = r(\rho t)$, $\rho \in (0, 1)$; this choice is necessary in some real situations, also to avoid actuator saturation and/or to ensure that the system to be controlled is not excessively forced.

*Remark 4:* If the model of the system (13) is not available, then it can be identified by using optimization algorithms based on experimental data (e.g., with the help of the MATLAB commands *invfreqs, armax*).

*Remark 5:* If $a_1$, $a_2$, $b$ of the system (13) depends on $y$, $v$, then the controller design can be performed via a Lyapunov approach by following the lines of the methods presented in [23] and [24].

## VII. DESIGN AND REALIZATION OF A CONTROLLER FOR AN ANTENNA SCANNING SYSTEM

Consider the horizontal motion of the antenna scanning system reported in Figs. 8 and 9. In details, Fig. 8 shows the scheme of the antenna scanning system. In particular, the antenna is mounted on the planar scanner. Only the horizontal motor is detailed, since the control system acts on the horizontal axis only. In such figure $r$ is the reference signal, $v$ is the velocity signal from the tachometer, $y$ is the position reading from the encoder and $u$ is the control signal feeding the power unit to control the scanner position.



FIGURE 8. Scheme of the antenna scanning system.

Fig. 9 is a photo of the antenna scanner detailing the horizontal axis sketched in Fig. 8. The probe mount can be seen on the left and the vertical axis also appears.

The planar scanner available at the Microwaves and Millimeter Wave Lab, University of Naples Federico II, is an MI Technologies (MI-3603-6X6) scanner.

From numerous experimental tests, the performance of the considered antenna scanning system with the controller designed and constructed by the manufacturer is acceptable only during the steady-state phase.

Based on the knowledge of the range of the applicable voltage values $u$, of the encoder and the tachometer data only, some experimental tests have been performed to identify the scanning system, by using a frequency domain approach



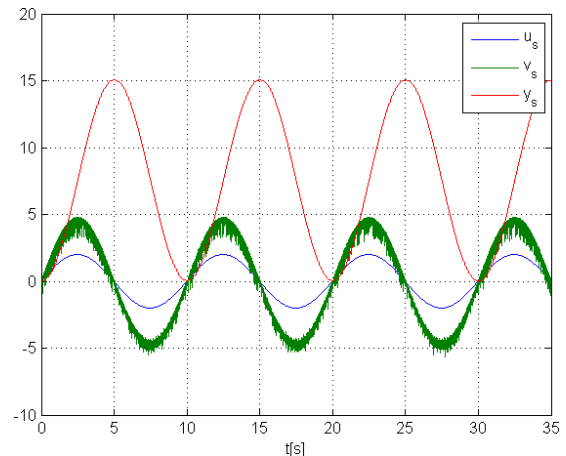FIGURE 9. Photo of the antenna scanner.



FIGURE 10. An experimental result for the identification.

(see Fig. 10) with the help of the MATLAB command *invfreqs*.

The identified model is (see Fig. 11)

$$W(s) = \frac{V(s)}{U(s)} = \frac{4890}{s^2 + 16.5s + 2070}. \quad (30)$$

By choosing $w = 60$ and $\varepsilon = 0$, from (25), it is:

$$K_d = 0.3338, \quad K_p = 6.1310, \quad K_i = 12.5860. \quad (31)$$

Note that the system to be controlled has high-frequency modes which are not identified and modeled. They are due to the elasticity of the transmission belt and to the cart carrying the antenna [30], [31]. Hence, to avoid any spillover phenomenon and possible high-frequency vibrations due to the noise amplification caused from the derivative action, a first-order filter is introduced downstream of the controller

$$W_f(s) = \frac{1}{1 + s\tau}. \quad (32)$$
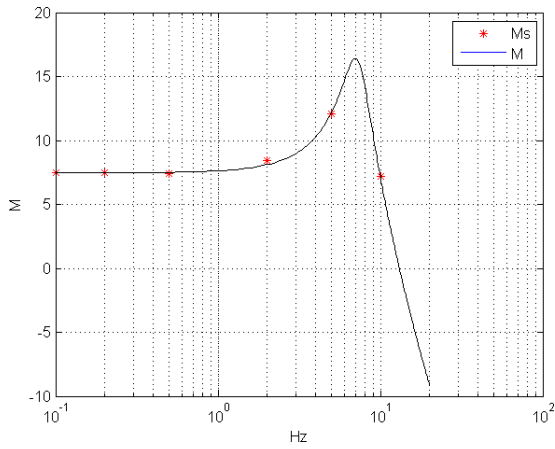
**IEEE** *Access*

A. Capozzoli *et al.*: Optimized Trajectory Tracking of a Class of Uncertain Systems Applied to Optimized Raster Scanning

**FIGURE 11.** $M_S$ experimental gain; M gain of the model (30).
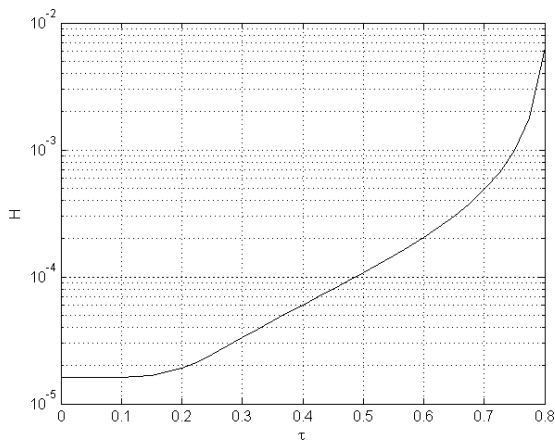


**FIGURE 12.** Variation of $H$ with respect to $\tau$.

In Fig. 12, the value of $H$ as a function of $\tau$ is plotted.

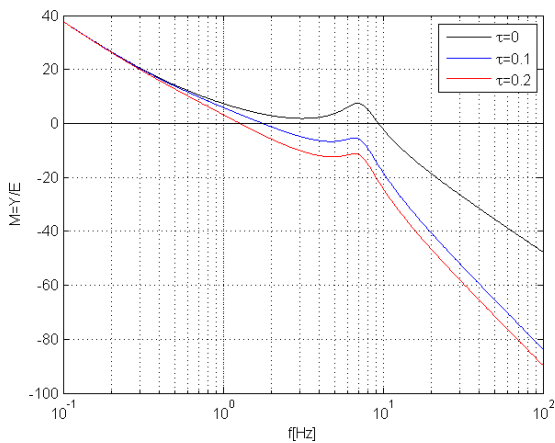Fig. 12 shows that the performance of the control system is reduced when $\tau$ increases until the system becomes unstable.



**FIGURE 13.** Open-loop frequency response for $\tau = 0, 0.1, 0.2$.

In Figs. 13 and 14, the open-loop frequency responses (error-position) and the closed-loop ones (reference



**FIGURE 14.** Frequency response reference-control for $\tau = 0, 0.1, 0.2$.
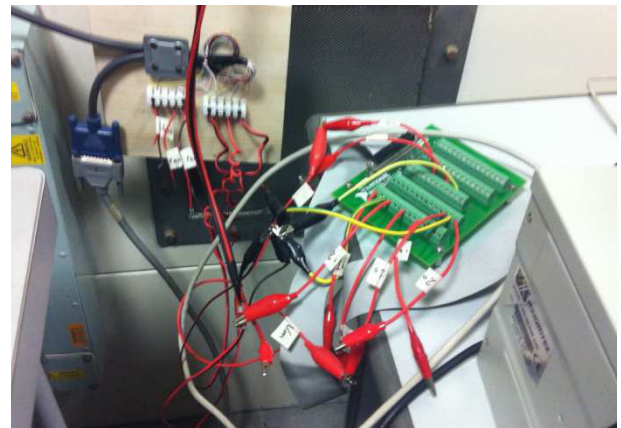




**FIGURE 15.** Configuration of the realized controller.

signal-control signal) are shown. These figures show the utility of the filter to eliminate the spillover phenomenon and the mitigation of the noise of the control signal.

The controller is designed with a filter that has $\tau = 0.1$, which has been realized by using an industrial HP PC equipped with a 16 bit input/output data acquisition board (National Instruments PCI-6035E) (see Fig. 15). The MATLAB Real-Time Windows Target has been used with a 20 kHz sampling frequency.
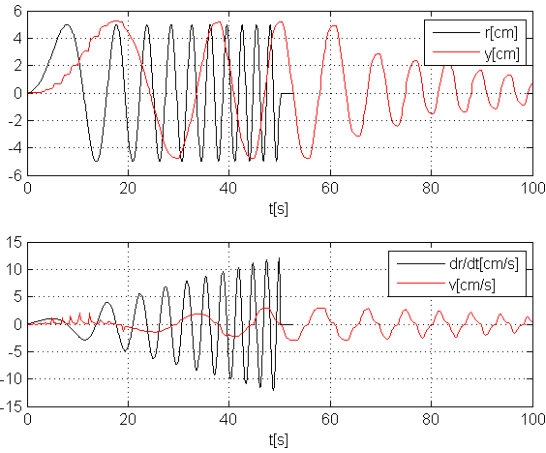
A. Capozzoli *et al.*: Optimized Trajectory Tracking of a Class of Uncertain Systems Applied to Optimized Raster Scanning

**IEEE** *Access*



**FIGURE 16.** Response of the antenna scanning system to a chirp signal with the current controller.



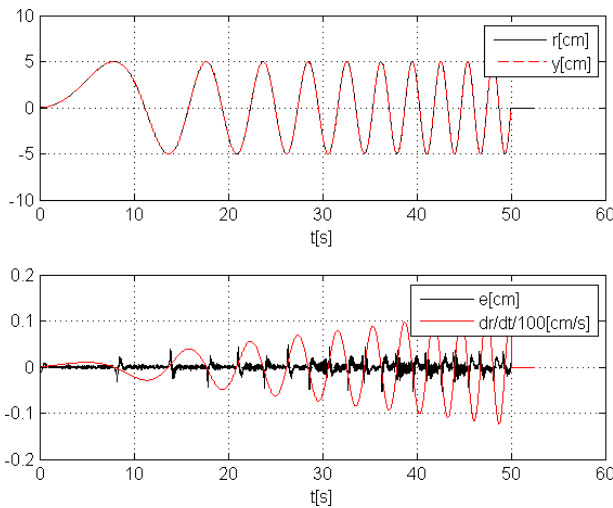**FIGURE 17.** Response of the antenna scanning system to a chirp signal by using the designed and realized controller.

In Fig. 16, the position of the antenna is reported for a chirp reference signal and by using the current controller.

In Fig. 17, the response of a chirp signal is plotted by using the designed and realized controller.

## VIII. APPLICATIONS

The first case considered is a *continuous scan* with a probe that moves during the measurement of the electromagnetic field. In the hypothesis that the measuring points are $y_k = 0, 2, 4, \cdots, 50cm$, the maximum velocity is $\hat{v} = 2cm/s$ and the maximum acceleration is $\hat{a} = 1.5cm/s^2$, the behaviors of $r, \dot{r}, \ddot{r}$ obtained by using Theorem 1, and the behavior of the computed error $e$, without compensation signal, are reported in Fig. 18. In Fig. 19, the actual error is shown in accordance with the computed one.

The second case considers a *stepped scan*, i.e., the probe is stopped (e.g., for 1 s) while measuring the electromagnetic field. It is assumed that the measuring points are $y_k = 0, 7, 16, 20, 30cm$, the maximum velocity is $\hat{v} = 2cm/s$
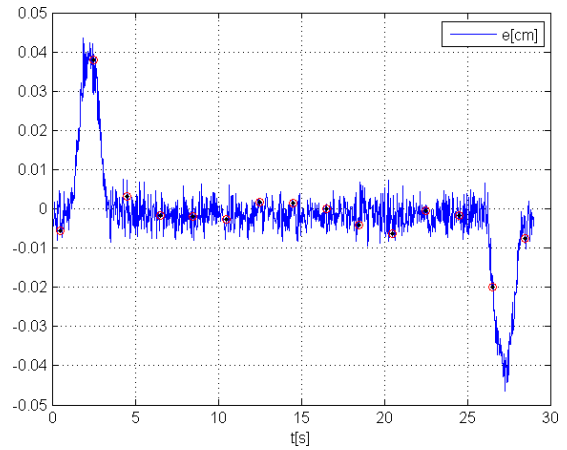


**FIGURE 18.** Time histories of $r, \dot{r}, \ddot{r}$ and of the computed error - continuous scan.



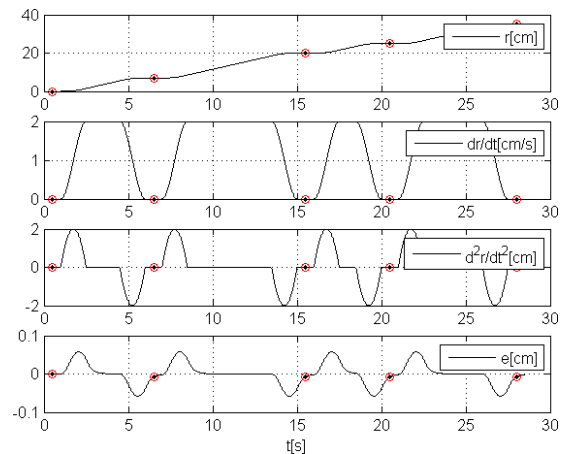**FIGURE 19.** Time history of the actual error – continuous scan.



**FIGURE 20.** Time histories of $r, \dot{r}, \ddot{r}$ and of the computed error – stepped scan.

and the maximum acceleration is $\hat{a} = 2cm/s^2$. Then the time histories of $r, \dot{r}, \ddot{r}$, obtained by using Theorem 1, and the time history of the computed error $e$, always without the compensation signal, are shown in Fig. 20. In Fig. 21, the actual error is reported in accordance with the computed one.
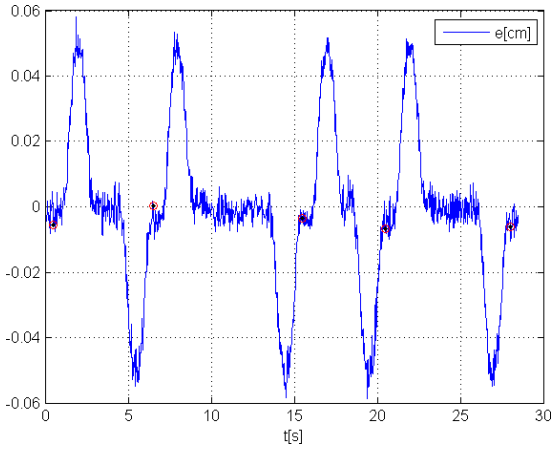
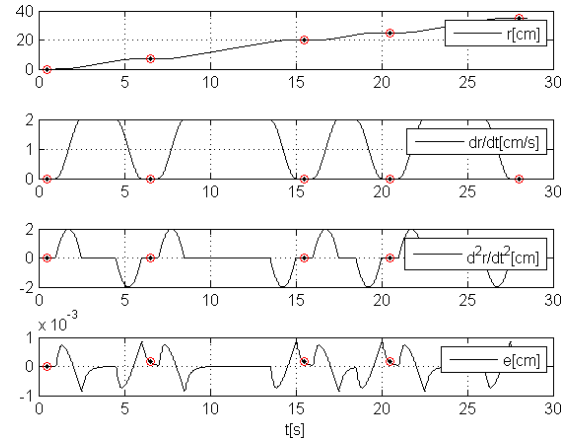**FIGURE 21.** Time history of the actual error – stepped scan.



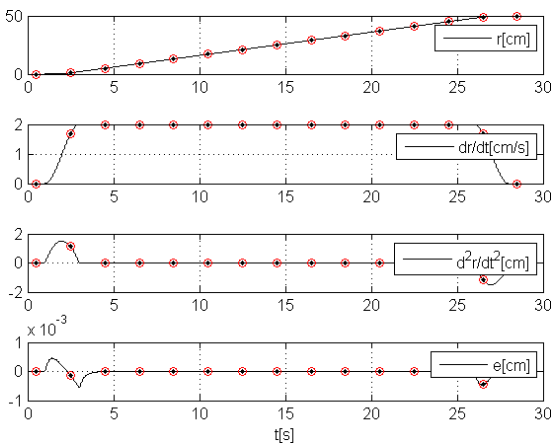**FIGURE 22.** Theoretical error with a compensation signal – continuous scan.



**FIGURE 23.** Experimental error with a compensation signal – continuous scan.



**FIGURE 24.** Theoretical error with a compensation signal – stepped scan.



**FIGURE 25.** Experimental error with a compensation signal – stepped scan.
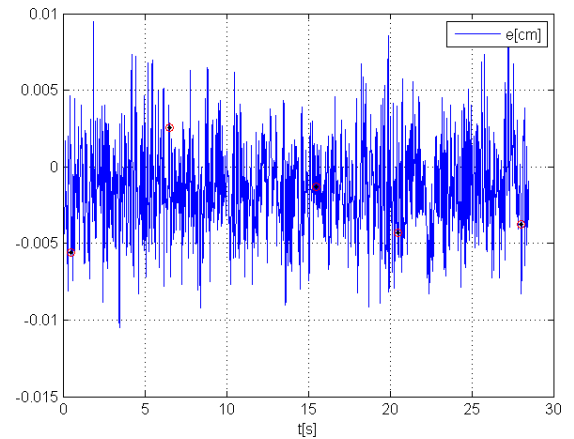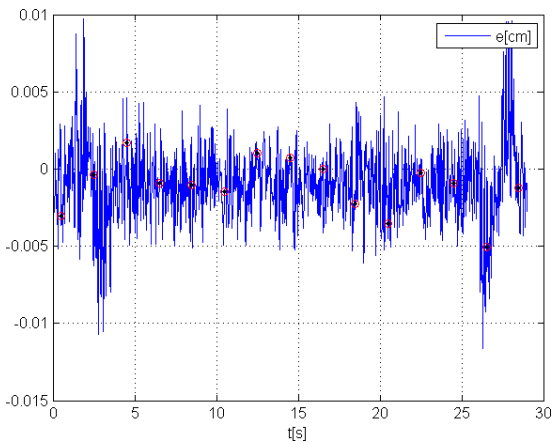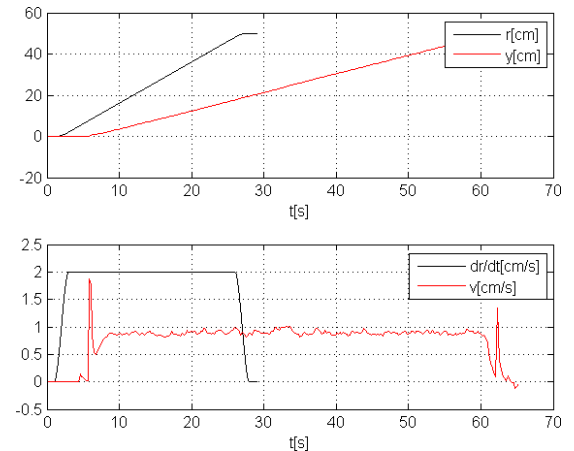


**FIGURE 26.** Response of the antenna scanning system by using the controller of the company – case: *continuous scan*.

In Figs. 22, 23, 24, 25 the performance of the antenna scanning system with the compensation signal $u_c = (a_2/b)$ $\dot{r} = 0.4233\,\dot{r}$ are reported.

Finally, in Figs. 26 and 27 the corresponding performance of the antenna scanning system by using the controller provided by the manufacturer are shown.

The third case considered is intended to illustrate how the synergy between the optimized NF sampling and the control system improves the performance. Experimental tests have been carried out to validate the performance.

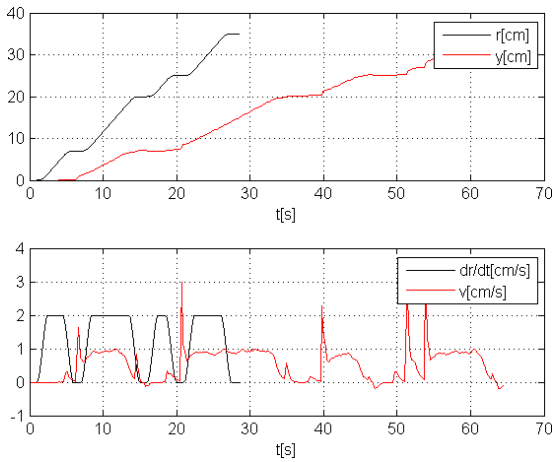The AUT is a double ridged broadband horn, Schwarzbeck BBHA 9120D with a $240 \times 140$ mm aperture and operating

A. Capozzoli *et al.*: Optimized Trajectory Tracking of a Class of Uncertain Systems Applied to Optimized Raster Scanning

IEEE*Access*

**FIGURE 27.** Response of the antenna scanning system by using the controller of the company – case: *stepped scan*.



**FIGURE 29.** Location of the optimized sampling points (red circles) and scanning path (blue line).

in the band 1-18 GHz. The test was performed at 9.5 GHz for $z_0 = 13\lambda$ (see Fig. 3). A picture of the measurement setup is shown in Fig. 28.
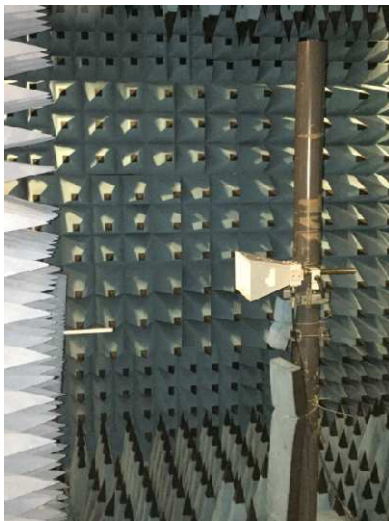


**FIGURE 28.** The measurement setup. The AUT is visible on the right, while the scanning probe is visible on the left.
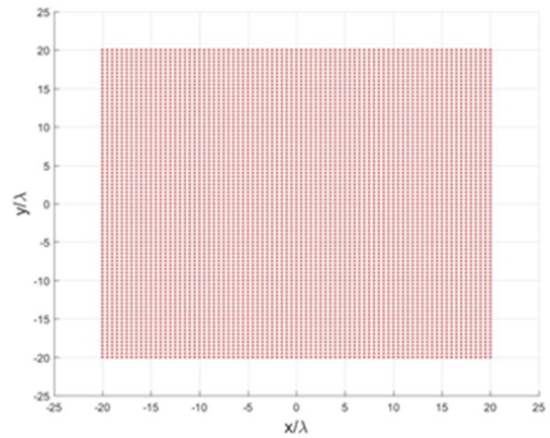


**FIGURE 30.** Standard sampling points distribution with $\lambda/2$ step.



**FIGURE 31.** Cut along the *u* axis of the reference FFP (blue line) and of the one reconstructed by using the presented approach (red pluses).

After the optimization process, a total of 458 samples were obtained with the distribution shown in Fig. 29 along the scanning path. The samples are arranged in horizontal rows so that the raster scan is straightforward.

A second NF data set was collected over a region of $20\lambda \times 20\lambda$ with a $\lambda/2$ step size to ensure that the comparison with the standard acquisition is possible. In this case, a total of 6561 points (shown in Fig. 30) is required to calculate the FFP.

Figs. 31 and 32 show the reconstructed FFP (red pluses) according to the optimized approach together with the one provided by the standard FFP (blue lines) along the principal cuts. The good agreement between the two different methods shows that the optimized grid can effectively provide the
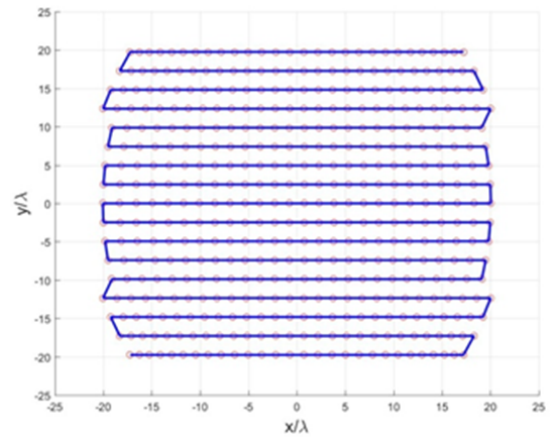
FFP of the AUT with the same accuracy as the standard approach.

To provide a reference for comparing the performance of the proposed control system, the optimized samples were

**IEEE**Access·

A. Capozzoli *et al.*: Optimized Trajectory Tracking of a Class of Uncertain Systems Applied to Optimized Raster Scanning
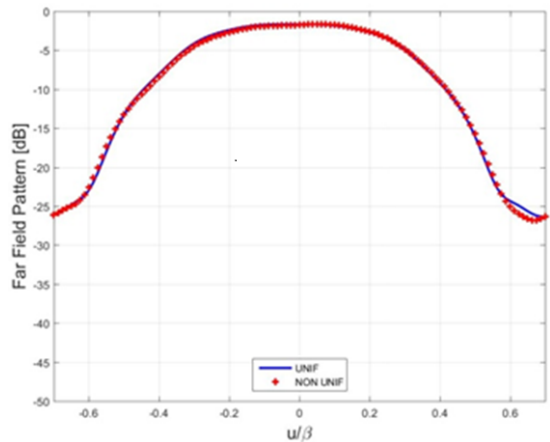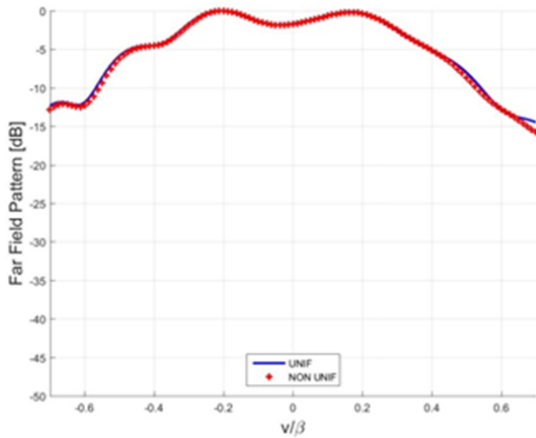


**FIGURE 32.** Cut along the *v* axis of the reference FFP (blue line) and of the one reconstructed by using the presented approach (red pluses).



**FIGURE 34.** Amplitude in dB of the NF sampled on a row of the optimized grid: standard scanning (blue line) and proposed scanning (red pluses).

also collected using a standard continuous raster scan with a constant scan velocity set equal to 1 cm/sec according to the VNA latency (Anritsu 37397C).

Thanks to the new control strategy, with a pseudo-trapezoidal velocity profile with $\hat{v} = 4cm/s$ and $\hat{a} = 8cm/s^2$ during the movement phase between two sampling points, the acquisition could be collected in 16 minutes, a time which is 2.5 times shorter than the time required for a standard scan. Clearly, a $\lambda/2$ sampling takes much longer due to the larger number of rows and could not profit significantly from the high performance of the controller due to the higher density of the sampling points.
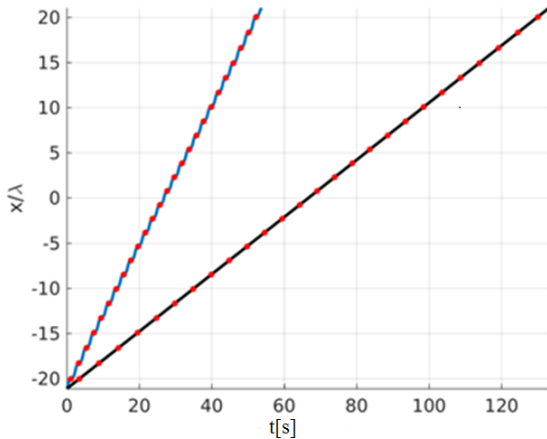


**FIGURE 35.** Phase in degrees of the NF sampled on a row of the optimized grid with the continuous scan (blue line) and the proposed controller (red pluses).

scan (red pluses). The agreement between these data shows that no significant errors are introduced by the smart control of the scanner.

## IX. CONCLUSION

In this paper, the optimized raster scanning for NF measurements has been introduced. The method significantly reduces the number of sampling points and the scanning path length. The dramatic reduction in the scanning time is achieved thanks to a smart controller. To this end, some theorems, that easily design a robust PID control law with a possible compensation signal without chattering, have been provided. They allow to force a very recurring class of uncertain systems to track sufficiently regular trajectories with a predetermined maximum error.

The proposed control law is easy to design and implement because it depends on only two design parameters: the first parameter is related to the precision of the tracking error, and the second is related to the robustness.

Some methods that generate references with bounded third derivatives have also been provided.



**FIGURE 33.** Scanning path of a single row with the proposed controller (blue line) and path with constant velocity (black line) along with the sampling points (red dots).

Fig. 33 shows the trajectory along a single row of the scanning for the proposed controller (blue line) and for the continuous scan (black line) along with the measurement points (red dots).

Figs. 34 and 35 show the NF along a row in terms of amplitude and phase, respectively. These data were acquired during the standard scan (blue line) and the proposed
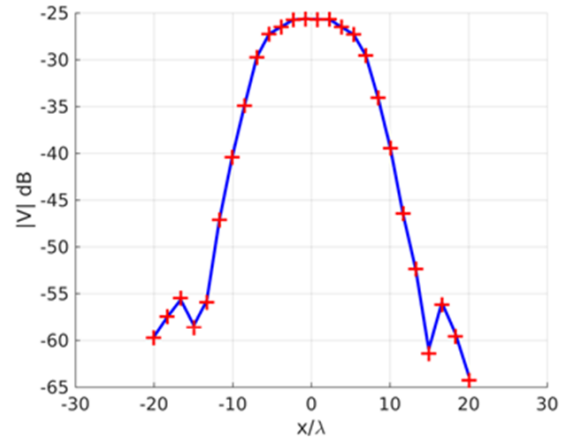
A. Capozzoli *et al.*: Optimized Trajectory Tracking of a Class of Uncertain Systems Applied to Optimized Raster Scanning

IEEE *Access*

By using the stated methodology, a high-performance controller of an antenna scanning system has been designed and realized. This system has been validated with numerous experimental tests and has been used much advantageously to make both continuous and stepped scans.

The authors are working to improve the current system also about the user interface.

## APPENDIX

*Lemma 1:* A fourth-order SISO linear, time-invariant system with transfer function

$$W(s) = \frac{1}{(s - p_1)(s - p_2)(s - p_3)(s - p_4)}$$
$$= \left( \frac{1}{(s - p_2)(s - p_2)\left[(s - \alpha)^2 + \omega^2\right]} \right), \quad (33)$$

i.e., without zeros and with four real poles (with two real poles $p_1$, $p_2$ and a pair of complex poles $\alpha \pm j\omega$, respectively), is externally positive (is externally positive iff $\alpha \le \max\{p_1, p_2\}$, i.e., iff at least a real pole does not lie to the left of the pair of complex poles in the complex plane, respectively).

*Proof:* See [21].

*Lemma 2:* Consider the system

$$e + d_1 e + d_2 \ddot{e} + d_3 \dot{e} + d_4 e = \zeta_p,$$
$$e(0) = \dot{e}(0) = \ddot{e}(0) = e(0) = 0. \quad (34)$$

If $W(s) = 1/(s^3 + d_1 s^4 + d_2 s^2 + d_3 s + d_4)$ is asymptotically stable and there exists a real number $\delta_p \ge 0$ such that $|\zeta_p| \le \delta_p$, then

$$|e(t)| \le H_p \delta_p, \quad H_p = \int_0^\infty |w(\tau)| \, d\tau, \quad w(\tau) = L^{-1}(W(s)). \quad (35)$$

Moreover, if $W(s)$ is also externally positive (the poles of $W(s)$ are $-\alpha, -\alpha, -\alpha \mp j\omega$), then

$$|e(t)| \le \frac{\delta_p}{d_4} \left( |e(t)| \le \frac{\delta_p}{\alpha^2(\alpha^2 + \omega^2)} \right). \quad (36)$$

*Proof:* Since $W(s)$ is asymptotically stable, from the implicit relation

$$e(t) = \int_0^t w(\tau) \zeta\left(t - \tau, e(t - \tau), \dot{e}(t - \tau)\right) d\tau, \quad (37)$$

it is

$$|e(t)| \le \int_0^t |w(\tau)| \, |\zeta| \, d\tau \le \int_0^\infty |w(\tau)| \, |\zeta| \, d\tau$$
$$\le \left( \int_0^\infty |w(\tau)| d\tau \right) \delta_p. \quad (38)$$

If $W(s)$ is also externally positive, then the system impulse response $w(\tau)$ is non-negative; hence

$$\lim_{t \to \infty} w_{-1}(t) = \lim_{t \to \infty} \int_0^t w(\tau) d\tau = H = \lim_{s \to 0} W(s) = \frac{1}{d_4}. \quad (39)$$

*Lemma 3:* Consider the system

$$e + d_1 e + d_2 \ddot{e} + d_3 \dot{e} + d_4 e = \dot{\zeta},$$
$$e(0) = \dot{e}(0) = \ddot{e}(0) = e(0) = 0. \quad (40)$$

If $W_p(s) = s/(s^3 + d_1 s^4 + d_2 s^2 + d_3 s + d_4) = sW(s)$ is asymptotically stable and there exists a real number $\delta \ge 0$ such that $|\zeta| \le \delta$, then

$$|e(t)| \le H_p \delta, \quad H_p = \int_0^\infty |w_p(\tau)| \, d\tau,$$
$$w_p(\tau) = L^{-1}(W_p(s)). \quad (41)$$

Moreover, if the poles of $W_p(s)$ are $-\alpha, -\alpha, -\alpha \mp j\omega$, then

$$|e(t)| \le \frac{\delta}{\alpha(\alpha^2 + \omega^2)}. \quad (42)$$

*Proof:* The inequality (40) is proven analogously to (36). To prove (41), since $w(t) = L^{-1}(W(s)) \ge 0$, then it easily follows

$$|w_p(t)| = \left| \frac{dw(t)}{dt} \right|$$
$$= \frac{d}{dt} \left| r_1 e^{-\alpha t} + r_1 t e^{-\alpha t} + r_3 e^{-\alpha t} \sin(\omega t + \beta) \right|$$
$$\le \alpha |w(t)|. \quad (43)$$

Finally, inequality (41) derives from (36) and (42).

## REFERENCES

[1] A. Yaghjian, "An overview of near-field antenna measurements," *IEEE Trans. Antennas Propag.*, vol. AP-34, no. 1, pp. 30–45, Jan. 1986.

[2] C. Parini, S. Gregson, J. McCormick, and D. J. Van Rensburg, *Theory and Practice of Modern Antenna Range Measurements*. London, U.K.: IEE, 2014.

[3] O. M. Bucci, C. Gennarelli, and C. Savarese, "Representation of electromagnetic fields over arbitrary surfaces by a finite and nonredundant number of samples," *IEEE Trans. Antennas Propag.*, vol. 46, no. 3, pp. 351–359, Mar. 1998.

[4] A. Capozzoli, C. Curcio, A. Liseno, and P. Vinetti, "Field sampling and field reconstruction: A new perspective," *Radio Sci.*, vol. 45, no. 6, p. RS6004, 2010, doi: 10.1029/2009RS004298.

[5] A. Capozzoli, C. Curcio, and A. Liseno, "Multi-frequency planar near-field scanning by means of singular-value decomposition (SVD) optimization," *IEEE Antennas Propag. Mag.*, vol. 53, no. 6, pp. 212–221, Dec. 2011.

[6] A. Capozzoli, C. Curcio, and A. Liseno, "NUFFT-accelerated plane-polar (also phaseless) near-field/far-field transformation," *Prog. Electromagn. Res. M*, vol. 27, pp. 59–73, Nov. 2012.

[7] A. Capozzoli *et al.*, "A probe-compensated helicoidal NF-FF transformation for aperture antennas using a prolate spheroidal expansion," *Int. J. Antennas Propag.*, vol. 2012, Jan. 2012, Art. no. 753156, doi: 10.1155/2012/753156.

[8] A. Capozzoli, C. Curcio, and A. Liseno, "Truncation in 'quasi raster' near-field acquisitions," *IEEE Antennas Propag. Mag.*, vol. 54, no. 5, pp. 174–183, Oct. 2012.

[9] F. D'Agostino, F. Ferrara, C. Gennarelli, R. Guerriero, and M. Migliozzi, "Reconstruction of the antenna far-field pattern through a fast plane-polar scanning," *Appl. Comput. Electromagn. Soc. J.*, vol. 31, no. 12, pp. 1362–1369, 2016.

[10] A. Capozzoli, C. Curcio, and A. Liseno, "Optimized spherical near-field antenna measurements," in *Proc. 8th Eur. Conf. Antennas Propag. (EuCAP)*, The Hague, The Netherlands, Apr. 2014, pp. 1685–1689.

[11] G. Ambrosino, G. Celentano, and F. Garofalo, "Tracking control of high-performance robots via stabilizing controllers for uncertain systems," *J. Optim. Theory Appl.*, vol. 50, no. 2, pp. 239–255, 1986.

[12] P. Dorato, Ed., *Robust Control*. Piscataway, NJ, USA: IEEE Press, 1987.

[13] S. Hara, T. Iwasaki, and D. Shiokata, "Robust PID control using generalized KYP synthesis: Direct open-loop shaping in multiple frequency ranges," *IEEE Control Syst.*, vol. 26, no. 1, pp. 80–91, Feb. 2006.

[14] B. Siciliano and O. Khatib, *Springer Handbook of Robotics*, 2nd eds. Cham, Switzerland: Springer, 2016.

[15] M. W. Spong and M. Vidyasagar, *Robot Dynamics and Control*. Hoboken, NJ, USA: Wiley, 2009.

[16] V. Utkin, J. Guldner, and J. Shi, *Sliding Mode Control in Electro-Mechanical Systems*. Boca Raton, FL, USA: CRC Press, 2009.

[17] T. Tuma, A. Sebastian, J. Lygeros, and A. Pantazi, "The four pillars of nanopositioning for scanning probe microscopy: The position sensor, the scanning device, the feedback controller, and the reference trajectory," *IEEE Control Syst.*, vol. 33, no. 6, pp. 68–85, Dec. 2013.

[18] G. Yang, J. Yao, G. Le, and D. Ma, "Asymptotic output tracking control of electro-hydraulic systems with unmatched disturbances," *IET Control Theory Appl.*, vol. 10, no. 18, pp. 2543–2551, 2016.

[19] V. Kumar, K. P. S. Rana, and P. Mishra, "Robust speed control of hybrid electric vehicle using fractional order fuzzy PD and PI controllers in cascade control loop," *J. Franklin Inst.*, vol. 353, no. 8, pp. 1713–1741, 2016.

[20] S. Zuo, M. Hughes, and G.-Z. Yang, "Flexible robotic scanning device for intraoperative endomicroscopy in MIS," *IEEE/ASME Trans. Mechatronics*, vol. 22, no. 4, pp. 1728–1735, Aug. 2017, doi: 10.1109/TMECH.2017.2700008.

[21] L. Celentano, "Tracking controllers design of references with bounded derivative," *Appl. Math. Sci.*, vol. 6, no. 95, pp. 4709–4728, 2012.

[22] L. Celentano, "Robust tracking method for uncertain MIMO systems of realistic trajectories," *J. Franklin Inst.*, vol. 350, no. 3, pp. 437–451, 2013.

[23] L. Celentano, "Design of a pseudo-PD or PI robust controller to track $C_2$ trajectories for a class of uncertain nonlinear MIMO systems," *J. Franklin Inst.*, vol. 354, no. 12, pp. 5026–5055, 2017.

[24] L. Celentano, "Pseudo-PID robust tracking design method for a significant class of uncertain MIMO systems," *IFAC-PapersOnLine*, vol. 50, no. 1, pp. 1545–1552, 2017.

[25] L. V. Kantorovich and G. P. Akilov, *Functional Analysis*. New York, NY, USA: Pergamon, 1982.

[26] P. C. Clemmow, *Plane Wave Spectrum Representation of Electromagnetic Fields*. Piscataway, NJ, USA: IEEE Press, 1996.

[27] A. Capozzoli, C. Curcio, and A. Liseno, "Regularization of residual ill-conditioning in planar near-field measurements," in *Proc. 10th Eur. Conf. Antennas Propag. (EuCAP)*, Davos, Switzerland, Apr. 2016, pp. 1–4.

[28] A. Capozzoli, C. Curcio, G. D'Elia, and A. Liseno, "Singular-value optimization in plane-polar near-field antenna characterization," *IEEE Antennas Propag. Mag.*, vol. 52, no. 2, pp. 103–112, Apr. 2010.

[29] A. Capozzoli, C. Curcio, G. D'Elia, and A. Liseno, "Phaseless antenna characterization by effective aperture field and data representations," *IEEE Trans. Antennas Propag.*, vol. 57, no. 1, pp. 215–230, Jan. 2009.

[30] L. Celentano and A. Coppola, "A wavelet based method to modeling realistic flexible robots," *IFAC Proc. Volumes*, vol. 18, no. Part 1, pp. 929–937, 2011.

[31] L. Celentano, "An innovative method to modelling realistic flexible robots," *Appl. Math. Sci.*, vol. 6, no. 73, pp. 3623–3659, 2012.

Award at the 8th European Conference on Antennas and Propagation in 2014. In 2015, he received a Senior Membership from AMTA. In 2016, he received the 2016 Best Italian EMC Poster Prize at the IEEE EMC Young Professional Paolo Corona Day.

He is a Founder and the Chair of the Italian AMTA Node and the first European Node of the ATMA. He is an Associate Editor of the *Express Journal of the Applied Computational Electromagnetic Society*.

Since 2016, he has been the Chair of the bachelor's and master's degrees in telecommunication engineering with the Università di Napoli Federico II, where he is also the Chair of the Microwave and Millimeter Wave Lab and the Numerical Electromagnetics Lab.

Since 2013, he has been responsible for the Course on Antenna Synthesis in the framework of the European School of Antennas (ESoA).

His research interests include, among others, methods to extract synthetic information on systems of sources or scatterers from field data, adaptive optics in optical astronomy, antenna synthesis and diagnosis, fast numerical methods in electromagnetics, GPU computing in electromagnetics, advanced measurement approaches in electromagnetics, inverse problems, and remote sensing.

**LAURA CELENTANO** has been an Assistant Professor of automation and control with the University of Naples Federico II and a Professor of the Fundamentals of Dynamical systems, Modelling and Simulation, and Automation of Navigation Systems, since 2006.

She has taught classes at the Italian Air Force Academy (Fundamentals of Dynamical Systems).

She has taken an active part in activities co-funded by the European Union, the Italian Ministry of University and Research, and the Economic Development, Region Campania, public and/or private corporations and industries.

She is an Author/Reviewer for the IEEE, ASME, ELSEVIER, and AIP journals and conferences.

She has been the chair and an organizer for conference sessions.

She has authored or co-authored scientific and educational books, presented by the IEEE Control Systems Society and international experts.

She is a Science Journalist and has cooperated with radio programs and journals on the popularization of scientific matters.

Her main research interests and activities include the design of versatile, fast, precise, and robust control systems of linear and nonlinear uncertain systems; methods for the analysis of stability and for the stabilization of linear and nonlinear uncertain systems (as well as MIMO and discrete-time systems); modeling and control of rigid and flexible mechanical systems; multi-valued control design methodologies; modeling and control of aeronautical, naval, and structural systems; rescue and security robotics; and telemonitoring and/or telecontrol systems.

**CLAUDIO CURCIO** received the Laurea degree (*summa cum laude*) in electronic engineering and the Ph.D. degree in electronic and telecommunication engineering from the Università di Napoli Federico II, Naples, Italy, in 2002 and 2005, respectively. From 2006 to 2007, he held a post-doctoral position with the University of Naples Federico II, where he is currently a Researcher. His main fields of interest are antenna measurements, standard and phaseless effective near-field/far-field transformation techniques, optical beamforming techniques for array antennas, and reflect-array synthesis.

In 2002, he was a recipient of the Optimus Award at the SIMAGINE 2002 Worldwide GSM & Java Card Developer Contest. In 2009 and 2010, he received the Best Technical Paper Award at the Antenna Measurement Techniques Association Symposium. In 2011, he was a recipient of the Honorable Mention for the Best Antenna Measurement Paper at the European Conference on Antennas and Propagation. In 2013, he was a finalist for the Antenna Measurements Best Paper Award at the European Conference on Antennas and Propagation. In 2016, he received the IEEE Best Italian EMC Poster Prize from the IEEE EMC Society, Italy Chapter.

**AMEDEO CAPOZZOLI** received the Laurea degree (*summa cum laude*) in electronic engineering and the Ph.D. degree in electronic engineering and computer science from the Università di Napoli Federico II, Naples, Italy. In 1999, he won the open national competition to earn a post as a Researcher at the Università di Napoli Federico II, where he has been an Associate Professor of electromagnetic fields since 2005.

He received the Telecom Italia Prize for the best thesis in electronic engineering at the Università di Napoli Federico II, the Barzilai Prize for Young Scientists from the Italian Society of Electromagnetism in 2002, the Best Technical Paper Award at the Antenna Measurement Technique Association (AMTA) for two consecutive years in 2009 and 2010, the Honorable Mention at the 5th European Conference on Antennas and Propagation in 2011, and the Nomination for the Best Paper

A. Capozzoli *et al.*: Optimized Trajectory Tracking of a Class of Uncertain Systems Applied to Optimized Raster Scanning

IEEE *Access*

**ANGELO LISENO** was born in Italy in 1974. He received the Laurea degree (*summa cum laude*) and the Ph.D. degree in electrical engineering from the Seconda Università di Napoli, Italy, in 1998 and 2001, respectively. From 2001 to 2002, he held a post-doctoral position with the Seconda Università di Napoli. From 2003 to 2004, he was a Research Scientist with the Institut für Hochfrequenztechnik und Radarsysteme of the Deutsches; Zentrum für Luft- und Raumfahrt, Oberpfaffenhofen, Germany. From 2005 to 2015, he was a Researcher with the Dipartimento di Ingegneria Elettrica e delle Tecnologie dell'Informazione, Università di Napoli Federico II, Napoli, Italy. Since 2015, he has been an Associate Professor with the Dipartimento di Ingegneria Elettrica e delle Tecnologie dell'Informazione.

His main fields of interest are parallel computing techniques for electromagnetics, general purpose GPU computing, complex and phaseless near-field/far-field transformation techniques, antenna synthesis, remote sensing, and inverse scattering and imaging.

Dr. Liseno received the Antenna Measurement Techniques Association Best Technical Paper Award in 2009 and 2010 and the Honorable Mention for the Best Antenna Measurement Paper at the European Conference on Antennas and Propagation in 2011, and was a finalist for the measurements Best Paper Award at the European Conference on Antennas and Propagation in 2013 and received the Best Italian EMC Poster Prize from the IEEE EMC Society, Italy Chapter, in 2016.

**SALVATORE SAVARESE** was born in Italy in 1988. He received the M.S. degree in electronic engineering (*summa cum laude*) from the University of Naples Federico II, Naples, Italy, in 2013, where he is currently pursuing the Ph.D. degree with the Dipartimento di Ingegneria Elettrica e Tecnologie dell' Informazione. In 2014, he held a scholarship position at the Istituto Nazionale di Astrofisica, Naples. His main research interests include diagnosis techniques for reflector antennas, antenna measurements, and computational techniques for electromagnetics.

● ● ●